LARGE EDDY SIMULATIONS OF FLOW AROUND A SMOOTH CIRCULAR CYLINDER IN A UNIFORM CURRENT IN THE SUBCRITICAL FLOW REGIME

Mia Abrahamsen Prsic [a, *], Muk Chen Ong [b], Bjørnar Pettersen [a], Dag Myrhaug [a]

[a] Department of Marine Technology, Norwegian University of Science and Technology, NO-7491 Trondheim, Norway

[b] Norwegian Marine Technology Research Institute (MARINTEK), NO-7450 Trondheim, Norway

ABSTRACT

Three-dimensional flow around a circular cylinder in a steady, uniform current at subcritical Reynolds numbers (Re) is investigated. The flow is simulated using Large Eddy Simulations (LES) with Smagorinsky subgrid scale model. Influences of various numerical parameters are investigated through the statistical values of the drag and the lift coefficients, Strouhal number, pressure distribution and separation angles, as well as through the flow field in the cylinder near wake.

The main purpose of the paper is to study the flow around a circular cylinder at Re=13100, which is chosen due to its applicability to the flow around cylindrical offshore structures in operational conditions, and because it belongs to a not thoroughly studied Re range. However, first the flow around a cylinder in the free stream at Re=3900 is investigated and the results are compared with numerous published results for validation of the chosen LES model. For the higher Re, the results are compared with the published experimental data and the numerical simulations for the similar flow regime. The chosen LES performs well. The results are in reasonably good agreement with previous studies and are discussed through standard hydrodynamic parameters and details of the flow around the cylinder and in the wake.

Keywords: circular cylinder; Large Eddy Simulations; Smagorinsky turbulence model; wake flow; subcritical Re.

* Corresponding author. Tel.: 0047 96 80 15 90; E-mail address: mia.prsic@ntnu.no (M. Abrahamsen Prsic)

Other authors, e-mail addresses: muk.chen.ong@marintek.sintef.no (M. C. Ong); bjornar.pettersen@ntnu.no (B. Pettersen); dag.myrhaug@ntnu.no (D. Myrhaug)

1. INTRODUCTION

Many offshore structures contain elements with cylindrical shape, such as jacket, jackup and tension-leg platforms, marine pipelines and bundles of marine risers. In the last 30 years, there has been a large increase in the use of such structures. Marine pipelines offer a sustainable and efficient way of oil and gas transportation. However, exposure to current and waves can cause the hazard of oil leakage. For safety issues it is important to broaden the understanding of the flow fields around such objects as well as the hydrodynamic loads exerted on them.

Pipelines at intermediate water depths are subjected to currents plus waves causing large variations in the velocities and thereby Reynolds number ($Re = U_c D/\upsilon$, where U_c is the free stream velocity, D is the diameter of the cylinder and υ is the kinematic viscosity of the fluid), most often appearing in the range from 10^3 to 10^7. It is therefore important to understand the flow around the circular cylinder in the actual Re range. In the present study, the moderate Re = 13100 is chosen, corresponding to standard operational conditions of marine pipelines and risers. Most of the published VIV (Vortex Induced Vibrations) experiments belong to the Re range between 500 and 60000 (Diana et al., 2008), comparable to the present Re. Zhang and Dalton (1996) performed Large Eddy Simulations (LES) in order to investigate VIV of a circular cylinder in steady flow for Re = 13000, very close to the Re targeted here. Two-dimensional (2D) simulations were performed. Even though the flow is turbulent and thus three-dimensional (3D), the test case presented for a steady circular cylinder provides reasonable comparison with the experimental results, leading to the conclusion that LES is a promising tool for such simulations. However, VIV studies would benefit from more accurate and thorough investigation of the steady state flow situation, as presented in this paper.

This study focuses on 3D modelling of the flow around a smooth circular cylinder in a steady current in the subcritical flow regime (Re = 13100). Validation of the code is done by

comparing the results for the benchmark case of the flow around a circular cylinder in the subcritical flow regime at Re = 3900 with numerous published experimental and numerical results. For the Re = 13100 case, details of the flow around, and in the near wake of the cylinder are analysed with respect to various numerical parameters, such as mesh resolution, time-step and computational domain size. The limitations of the measuring equipment used in some published experiments lead to difficulties in capturing the details of the flow, especially in the near wake. Therefore the present paper also focuses on describing the flow near the body surface and in the cylinder near wake.

Recently published numerical results are mainly based on LES. Breuer (1998 a, b) made a detailed analysis of the influence of the subgrid scale models, the grid resolution and the discretization schemes on the quality of the LES results. Tremblay et al. (2002) carried out a series of LES and compared them with the results of Direct Numerical Simulations (DNS). Wissink and Rodi (2008) used DNS and presented the details of the flow field in the near wake of a circular cylinder at Re = 3300. Parnaudeau et al. (2008) focused on the comparison of their LES results with the experimental results obtained by Particle Image Velocimetry (PIV). Krajnovic (2011) used LES with Smagorinsky subgrid scale model to simulate the flow around a vertical cylinder at Re = 20000. Lysenko et al. (2012) performed LES with standard Smagorinsky and k-equation eddy viscosity model for the compressible fluid at Re = 3900 and low Mach number. Based on the previously mentioned research, LES is chosen as a promising numerical tool for simulating the flow behind a bluff body. In this paper, results are compared and discussed through the hydrodynamic quantities, such as drag and lift coefficients, Strouhal number, pressure and velocity distribution around the cylinder, and flow field in the near wake of the cylinder.

Experimental data for the flow around a fixed circular cylinder is available mostly for either very low or very high Re flows. Early measurements are documented by Linke (1931) and Thom (1928), mainly discussing the pressure distribution around the cylinder measured in a wind tunnel.

Roshko (1961) focused on Re from 10^6 to 10^7, as well as collecting and analysing data from many previous measurements considering subcritical Re. Schewe (1983) carried out a series of experiments in a pressurized wind tunnel, from subcritical to transcritical flow with Re from 2.3 * 10^4 to 7.1 * 10^6. Cantwell and Coles (1983) studied experimentally the near wake flow field of a circular cylinder at Re = 1.4 * 10^5. Norberg (1994) focused on investigating the Strouhal number and the base suction coefficient behind the cylinder at Re between 50 and 4 * 10^4. More experimental data was obtained by hot-wire and x-ray probe measurements of the near wake flow behind the circular cylinder by Ong and Wallace (1996) at Re = 3900.

The numerical research of the flow with comparable Re is limited, while the higher Re cases are studied in several publications. Fang and Han (2011) made a short discussion of the numerical results for the flow at three different moderate Re (5.6 * 10^3, 2.8 * 10^4 and 1.1 * 10^5); Ouvrard et al. (2008) published hybrid RANS/LES data for Re = 1.4 * 10^5; Breuer (2000) explored the influence of the various turbulence closure schemes and mesh refinements on the LES results for Re = 1.4* 10^5; Vaz et al. (2007) explored the influences of the numerical parameters and the different turbulence models in 2D and 3D simulations at Re = 9 * 10^4 and 5 * 10^6. In the higher Re range, Catalano et al. (2003) presented LES results with wall stress model for Re = 5 * 10^5 and 10^6; Ong et al. (2009) used 2D Unsteady Reynolds-Averaged Navier-Stokes (URANS) equations with a k – ε turbulence model for Re in the range 10^6 to 3.6 * 10^6; Lin et al. (2011) also used the k – ε turbulence model to explore the influence of various advection schemes on the drag coefficient for Re = 10^6.

In this paper, a short overview of the chosen numerical method is presented in the following Section. Details of the numerical simulations are presented in Section 3. The results are discussed in Section 4, including the analysis procedure, the validation study for the Re = 3900 flow, the convergence study for the Re = 13100 cases and the comparison with previously published results.

2. NUMERICAL METHOD

A LES model is chosen due to its capability of modelling the moderate high Re flow and resolving the 3D bluff body flow in a less numerically costly manner than DNS. In a LES model, the large scale turbulence is simulated directly and the subgrid scale turbulence, which is assumed to behave more case independent, is modelled.

In order to simulate the flow, the incompressible Navier-Stokes equations need to be solved. In the filtered form, the continuity and the momentum equations, disregarding the commutation error, can be written as:

$$\frac{\partial \bar{u}_i}{\partial x_i} = 0 \tag{1}$$

$$\frac{\partial \bar{u}_i}{\partial t} + \frac{\partial (\bar{u}_i \bar{u}_j)}{\partial x_j} = -\frac{1}{\rho}\frac{\partial \bar{p}}{\partial x_i} + \nu \frac{\partial^2 \bar{u}_i}{\partial x_j^2} - \frac{\partial \tau_{ij}}{\partial x_j} \tag{2}$$

where $u_{i,j}$, i, j∈[1, 2, 3] denotes the filtered velocity component in streamwise (x), crossflow (y) and spanwise (z) direction respectively, see Figure 2. x_i is assigned to the respective directions, ρ is the density of the fluid, p is the filtered pressure and τ_{ij} represents the non-resolvable subgrid stress, given by:

$$\tau_{ij} = \overline{u_i u_j} - \bar{u}_i \bar{u}_j \tag{3}$$

The commonly used Smagorinsky subgrid scale model (Smagorinsky, 1963) is based on the Boussinesq approximation, assuming that the turbulence stresses behave in the same manner as the large scale strain rate tensor S_{ij} :

$$\tau_{ij} - \frac{1}{3}\delta_{ij}\tau_{kk} = -2\nu_t \bar{S}_{ij} \tag{4}$$

where δ_{ij} denotes the Kronecker delta and ν_t is the subgrid scale eddy viscosity. The strain rate tensor S_{ij} in the resolved field can be written as:

$$\bar{S}_{ij} = \frac{1}{2}\left(\frac{\partial \bar{u}_i}{\partial x_j} + \frac{\partial \bar{u}_j}{\partial x_i}\right) \tag{5}$$

The subgrid scale eddy viscosity ν_t is a function of the strain rate tensor and the subgrid length l :

$$\nu_t = l^2|\bar{S}_{ij}| \tag{6}$$

$$l = C_s\bar{\Delta} \tag{7}$$

$$|\bar{S}_{ij}| = \sqrt{2\bar{S}_{ij}\bar{S}_{ij}} \tag{8}$$

The filter width Δ is correlated to the typical grid spacing by the cube root of the cell volume. C_s is the Smagorinsky constant with a value of 0.2 in the present study. More sophisticated subgrid scale models have been developed, such as the dynamic Smagorinsky model (Germano et al. (1991), Lilly (1992)) in which C_s becomes a so called dynamic constant, a local, time-dependent variable determined from the resolved velocity field.

Breuer (1998 a, 2000), Tremblay et al. (2002) and Lysenko et al. (2012) discussed the advantages and the differences of various subgrid scale models. Breuer (1998 a) analysed the simulations performed with the same numerical set-up, but without any subgrid scale model, with standard and with dynamic Smagorinsky model. He concluded that, in comparison to relatively large influence of the various discretization schemes, the subgrid scale models have a relatively small influence. While the simulation without any subgrid scale model showed the shortest recirculation length, the results obtained with Smagorinsky and dynamic Smagorinsky models were close to each other and showed better agreement with experimental results. Standard Smagorinsky model yielded a 2.5% larger drag coefficient, 0.2% larger primary separation angle and 1.25% smaller secondary separation angle compared with the dynamic Smagorinsky model. Through comparison of several flow parameters, Lysenko et al. (2012) discussed the differences between the standard Smagorinsky and the dynamic k-equation eddy viscosity (TKE) model. They concluded that the results obtained with Smagorinsky model compared well with the experimental results by Lourenco and Shih (1993), while the TKE results compared better with the results of Parnaudeau et al. (2008). Lysenko et al. (2012) also calculated the one-dimensional energy spectra of simulations

with Smagorinsky and TKE model. Both sets of data showed good agreement with experimental results of both Ong and Wallace (1996) and Parnaudeau et al. (2008). The spectra obtained by Smagorinsky model showed to be less dissipative than those obtained by TKE. Taking these results into account, it can be concluded that, even though the dynamic models are less rigid, a standard Smagorinsky model gives comparable quality of the results. It is also commonly used in the established cases for the flow around the circular cylinder for Re = 3900. For the sake of simplicity and comparability, a standard Smagorinsky model is chosen in this work.

All the simulations are performed using the open source code OpenFOAM, a computational fluid dynamics solver with extensive libraries for turbulence modelling. It is a finite volume code written in C++ using object-oriented techniques (OpenFOAM, 2011). Advantages of LES modelling in OpenFOAM can be explored through an example similar to the topic discussed in this paper, i. e. flow around a square cylinder, made by the code creators (Weller et al., 1998).

The PISO algorithm (Pressure Implicit with Splitting of Operators), described by Ferziger and Peric (2001), is used to solve the Navier-Stokes equations. A preconditioned conjugate and bi-conjugate method with diagonal incomplete-Cholesky (for symmetric) and diagonal incomplete-LU (for asymmetric matrices) are used for solving linear systems (OpenFOAM, 2011). For the time integration, an implicit, backward differencing method of second order is chosen, also used by Lysenko et al. (2012). Spatial schemes for the convective term approximations and inviscid terms are Gauss linear and Gauss limited linear. Those are central differencing schemes with a standard finite volume discretization of Gaussian integration which requires the interpolation of values from the cell centres to the face centres. All of the above schemes are of second order accuracy, which is, as summarized by Krajnovic (2011), the most common in engineering applications of LES. Discussion of the influences of the various numerical methods can be found in Breuer (1998 b). He compared various discretization schemes for the convective terms, such as a combination of upwind and a central differencing scheme, a central differencing scheme of second and fourth order, a

hybrid linear/parabolic scheme and a parabolic second order approximation. It was shown that the central differencing schemes offered the best agreement with the experiments. Even though the fourth order schemes yielded slightly better results, the variations between the central schemes of second and fourth order were much smaller than among other schemes. Therefore it is considered that the second order discretization schemes offer a good option for LES.

3. COMPUTATIONAL MODEL

The size of the 3D computational domain for the majority of the cases is 32D * 16D * 4D (x, y, z). The centre of the cylinder (and the origin of the coordinate system) is placed 8D from the inlet boundary, 8D away from the top and the bottom boundaries and 24D away from the outlet boundary (Figure 1). Simulations with both 4D and 8D spanwise (z) domain width are made for Re = 13100 to study the effect of the spanwise length.

For the simulations of the flow with Re = 3900, the domain size is chosen by comparison with the established standards for this benchmark case. Both Parnaudeau et al. (2008) and Tremblay et al. (2002) extended their domains over the same area: 20D in the streamwise (x) and crossflow (y) directions, while the centre of the cylinder was placed 5D downstream from the inlet boundary. The spanwise length of the domains in the aforementioned papers was πD. Franke and Frank (2002) used a slightly larger domain extending over 10D in front of the cylinder, 20D behind and 10D above and below the cylinder. Their domain also had a spanwise length of πD. Breuer (1998 b) used a circular domain with a radius of 15D and πD spanwise length. Wissink and Rodi (2008) used a 25D * 20D * 4D domain, Li (2011) used a smaller domain size of 27D * 9D * 2.3D, while Heggernes (2005) used exactly the same domain size as chosen in the present paper. Considering the aforementioned dimensions, the chosen domain size is assumed to be sufficient to obtain results unaffected by the boundary conditions.

In the Re = 13100 case, the same domain size is used. Since there is not many numerical

simulations published at this Re, the domain size is compared with the higher Re simulations. Ong et al. (2009) simulated the flow at very high Re, using two-dimensional k-ε URANS. Their domain spreaded over 7D in front of, above and below the circular cylinder and 20D behind the cylinder. Breuer (1998 b and 2000) used a a cylindrical domain with a radius of 15D and a somewhat smaller spanwise length of 2D and πD for LES at both Re = 3900 and 140000. Fang and Han (2011) used a domain of 28D * 8D * 10D for all their Re. Based on the fact that smaller domains have successfully been used for simulations of the flow at higher Re, the computational domain used in this work is considered to be sufficiently large.

In order to obtain results independent of the mesh, it is important to take shape, resolution and distribution of the elements into consideration. To avoid possible spurious oscillations and numerical instabilities, attention is paid to the smoothness of the transitions between adjacent mesh patches. In this case, a symmetric, body-fitted hexahedron mesh is divided into several zones. A small, O-shape zone of 0.2D width (Zone 1) is created around the cylinder in order to provide easier control of the cell sizes in the immediate vicinity of the cylinder. A second zone of O-shape mesh (Zone 2) extends up to 5D radially from the cylinder centre. The outermost part (Zone 3), between the outer edge of Zone 2 and the domain boundaries is filled with slightly radially stretched hexahedron elements. Finally, Zone 4 in the far wake of the cylinder consists of a coarser, rectangular mesh, slightly clustered towards the centre of the domain. Figure 2 presents the visualization of the entire domain, Zones 1- 4 and a more detailed view of Zones 1 and 2 near the cylinder. Meshes of the same distribution, i.e. the same shape of the elements in respective Zones, with different number of elements and mesh refinements are used in all the cases for both Re.

The boundary conditions are kept the same throughout the entire study. At the inlet, a uniform and constant velocity is prescribed. At the outlet, the pressure and the normal gradient of the velocities are set to zero. The top, bottom and side boundaries are considered to be free-slip surfaces, utilizing a symmetry boundary condition, while a no-slip condition is applied on the

cylinder surface. The influence of the boundary conditions is discussed in Section 4.

Five simulations are carried out at Re = 3900, with inlet velocity U_c = 0.39 m/s. The dimensionless time-step $\Delta t = 0.0008$ is chosen to keep the maximum Courant number below 0.6 (see Table 1, for other details of the simulations). The Courant number is defined as $C = U_{abs} \Delta t/\Delta\delta$, where U_{abs} is the magnitude of the velocity through the cell and $\Delta\delta$ is the cell size in the direction of the velocity. In all the simulations the element size on the surface of the cylinder is kept the same and is chosen in such a manner that the maximum dimensionless wall distance δ^+ is kept below 1. Here δ^+ is defined as $\delta^+ = u_* \delta/\nu$, where u_* denotes the friction velocity at the nearest wall, and δ is the normal distance from the wall. The maximal values of dimensionless streamwise wall distance, x^+, are smaller than 2 for all simulations, in the cross-flow direction, $y^+ < 4.5$ and in the spanwise direction, $7 < z^+ < 26$; x^+, y^+ and z^+ are defined according to Krajnovic (2011) as $x^+ = u_*\xi/\nu$; $y^+ = u_*\iota/\nu$; $z^+ = u_*\zeta/\nu$, where ξ, ι and ζ are the distances from the wall in x, y and z direction, respectively.

The difference between four of the simulations for Re = 3900 is the mesh refinement, especially in the near wake of the cylinder (Zones 1 and 2). The mesh refinement is performed radially and along the circumference of the cylinder in order to keep the shape and ratios of the elements as constant as possible. The 3900_m4 case is performed with the finest mesh of 13.5 million elements. In the 3900_m3 case, the 3D computational domain contains approximately 11 million elements; in the 3900_m2 case, 8 million elements are used; and in the 3900_m1 case, 5 million elements are distributed over the computational domain. The fifth simulation, the 3900_pbc case, is performed with the finest mesh, analogous to the 3900_m4 case, but with periodic boundary condition on the side boundaries, in order to check the influence of the boundary condition on the results.

Eight simulations are carried out for the flow around the circular cylinder at Re = 13100 in order to explore the influence of the mesh refinement in the near wake zone, the domain size, the time-step and the spanwise mesh resolution (details are presented in Table 2). The results are

discussed in the following Section.

TABLE 1: Numerical set-up for the Re = 3900 cases: the domain size is 32D * 16D * 4D; the number of elements spanwise is 150.

Case	Num. elem. (million)	Num. elem. circumf.	Boundary condition in the spanwise direction
3900_m1	5	340	free-slip
3900_m2	8	400	free-slip
3900_m3	11	480	free-slip
3900_m4	13.5	540	free-slip
3900_pbc	13.5	540	periodic

TABLE 2: Numerical set-up for the Re = 13100 cases.

Case	Domain (*D)	Number elem. (million)	Num. elem. spanwise	Num. elem. circumf.	Δt (s)
13100_m1	32 * 16 * 4	2	100	244	0.0001
13100_1	32 * 16 * 4	4.3	100	340	0.0001
13100_m2	32 * 16 * 4	7.7	100	480	0.0001
13100_m3	32 * 16 * 4	11	100	540	0.0001
13100_t2	32 * 16 * 4	4.3	100	340	0.0002
13100_t3	32 * 16 * 4	4.3	100	340	0.0004
13100_sm	32 * 16 * 4	6.5	150	340	0.0001
13100_sl	32 * 16 * 8	8.6	200	340	0.0001

4. RESULTS AND DISCUSSION

4. 1. ANALYSIS PROCEDURE

The details of the flow around the circular cylinder are presented with emphasis on the near-wake flow. The overall features of the flow are represented by the drag and lift coefficients and the Strouhal number. The details of the near-wake flow are explored through the velocity field in the wake, the recirculation length, the pressure coefficient distribution around the cylinder and the separation angles. Here, the drag coefficient is defined as $C_d = F_d/(0.5\rho U_c^2 A)$, where F_d is the drag force obtained by integrating over the cylinder surface. A is the frontal area of the cylinder. The lift coefficient is $C_l = F_l/(0.5\rho U_c^2 A)$, where F_l is the integrated lift force. The pressure coefficient is $C_p = (p'-p_\infty)/(0.5\rho U_c^2)$ where p' is the pressure at the sampling point and p_∞ is the pressure in the undisturbed flow. Time-averaging is made for a fully developed flow. The Re = 3900 cases are averaged over more than 50 vortex shedding cycles and the Re = 13100 cases over between 130 and 190 vortex shedding cycles.

As mentioned before, a free-slip boundary condition is assigned to the lateral planes of the domain. It has been successfully used by Krajnovic (2011), but it implies a non-physical requirement of zero normal velocity at the boundary plane. Therefore it is presumed that a certain

layer of the fluid in the vicinity of the lateral boundaries is influenced by this boundary condition and is thus excluded from the analysis. To check the influence of the boundary condition, the time-averages of the wall-normal velocity component are calculated at several cross sections in the cylinder wake, 0.53D, 0.7D, 1D and 2D from the cylinder centreline in the (x, y) plane. The absolute values of the time-averaged wall-normal velocities are further averaged along the cylinder, covering various spans from the cylinder centre towards the boundaries. The time-averaged wall-normal velocity is expected to be nearly constant and approaching zero along the boundary-unaffected part of the cylinder. Therefore the flow is considered affected as soon as the space-averaged values begin to change when averaged over wider spans. Figure 3 shows the time-averaged wall-normal velocity component for the 13100_1 case, indicating that the influence of the boundary condition is strongest in the immediate wake of the cylinder (x/D = 0.53). It appears as an increase in the absolute value of the wall-normal velocity component in the vicinity of the boundaries (close to z/D = 0 and 4). The analysis has been made for all Re = 3900 and Re = 13100 cases. It is concluded that the time- and space-averaged wall-normal velocities remain nearly constant for the central 2.4D part of the 4D long cylinder and for the 6.4D of the 8D long cylinder (the 13100_sl case). Therefore, in the following analyses, space-averaging is made only along the central 2.4D and 6.4D of the cylinder.

The influence of the alternative choice for boundary condition on the lateral boundaries is checked through two simulations for Re = 3900. While the 3900_m4 case is performed with the free-slip boundary condition, the 3900_pbc case is simulated using all numerical parameters the same except the periodic boundary condition on the lateral boundaries. The results are compared in Figure 4, through the time- and space-averaged streamwise velocity component, averaged in the above described manner for both simulations. Slight differences can be noticed between 3D and 6D in the cylinder wake, but they do not exceed 2%. It is therefore concluded that the free-slip boundary condition can be used for this kind of simulations, as long as attention is paid on the

space-averaging.

4.2. VALIDATION STUDY - REYNOLDS NUMBER 3900

4. 2. 1. Hydrodynamic quantities

A grid convergence study is performed for the flow at Re = 3900 through four simulations, varying the number of the elements and by comparing with numerical results by Breuer (1998 a), Franke and Frank (2002), Tremblay et al. (2002) and Lysenko et al. (2012) and experimental results by Lourenco and Shih (1993), Ong and Wallace (1996) and Parnaudeau et al. (2008). The Strouhal number ($St = f D/U_c$, where f is the vortex shedding frequency) is obtained from the power spectra of the lift force fluctuations, following the procedure of Schewe (1983). As seen from Table 3, St = 0.2152 for the two cases with the finest mesh (3900_m4 and 3900_m3), and that compares well with the results of the aforementioned authors. Figure 5 shows C_d (time- and space-averaged values of the drag coefficient) and $C_{l\ rms}$ (the root-mean-square (rms) value of the lift coefficient). The results in Figure 5 are given for simulations using 5, 8, 11 and 13 million elements, respectively. Conclusions drawn from Figure 5, Table 3 and the good agreement of C_d and $C_{l\ rms}$ of the 3900_m4 case with the previously published results (Table 4) suggest that the convergence is approached.

TABLE 3: Mean flow parameters for the Re = 3900 cases.

Case	C_d	$C_{l\ rms}$	St
3900_m1	1.2365	0.4490	0.2054
3900_m2	1.1483	0.2887	0.1956
3900_m3	1.0859	0.2163	0.2152
3900_m4	1.0784	0.1954	0.2152
3900_pbc	1.1102	0.2596	0.2152

4. 2. 2. Flow in the cylinder wake

Further validation is made by analysing the details of the flow in the cylinder wake and comparing with previously published data. Several cross sections perpendicular to the cylinder axis are considered and the data is averaged in the spanwise (z) direction and in time. The velocity field is sampled along the x-axis (see Figure 1) and over a vertical cross section parallel to the y-axis. In both cases, the velocity field is sampled over cross sections distributed evenly along the cylinder axis, excluding a length of 0.8D from each end of the cylinder. For sampling along the x-axis, the sampling sections are located at the cylinder centreline, i. e. in the (x, z) plane starting from x/D = 0.5, y/D = 0 and covering eight diameters downstream. Figure 6 shows the time- and space-averaged values of the streamwise velocity component (u) in the (x, z) symmetry plane of the cylinder wake for all four simulations. The 3900_m4 and 3900_m3 cases obtain the velocity minima positioned farthest away from the cylinder, while 3900_m1 and 3900_m2 have shorter wake disturbances (see the region between x/D = 0.5 and 3 in Figure 6). Even though the 3900_m4 case obtains a somewhat less pronounced minimum, the velocity profiles in the wake, especially at x/D > 1.5 show the smallest relative differences.

The mean dimensionless recirculation length (L_r) is defined as the distance between the base of the cylinder and where the sign of the centreline mean streamwise velocity component changes, divided by D. For the coarsest mesh, L_r obtains value of 0.96, corresponding to 25% shorter recirculation length than for the finest mesh. As previously concluded from Figure 6, the finer meshes yield longer wakes, leading to L_r = 1.27 for the 3900_m4 case. The L_r difference for the two finest meshes is 6%.

In Figure 7 a and b, the results of the 3900_m4 case are compared with previously published numerical and experimental results, generally showing good agreement. The present mean streamwise velocity profiles in the cylinder mid-plane (Figure 7 a) compare very well with the experimental results of Lourenco and Shih (1993) and Ong and Wallace (1996); in the near wake

also with the DNS results by Tremblay et al. (2000). However the results show more discrepancy from the results by Parnaudeau et al. (2008) and Lysenko et al. (2012) obtained with a TKE subgrid scale model. Similar behaviour is noticed by Lysenko et al. (2012) who, through comparison of several flow parameters, concluded that LES with Smagorinsky model yields results in good agreement with the PIV results of Lourenco and Shih (1993), while the TKE model leads to better agreement with the experiments of Parnaudeau et al. (2008). Figure 7 b shows the mean streamwise velocity component in the vertical (y, z) plane in the near wake of the cylinder. A characteristic V-shaped velocity profile is observed; and the results are in good agreement with the numerical results of Tremblay et al. (2000) and the experiments of Lourenco and Shih (1993).

There are significant differences in published values for the mean recirculation length at Re = 3900 (Table 4). Parnaudeau et al. (2008) presented a detailed discussion about the sensitivity of L_r with respect to the time averaging interval. The conclusion was that the fully converged value of L_r could not be obtained for less than 250 vortex shedding cycles. The uncertainty associated with shorter averaging periods was roughly estimated to ±12% for averaging over 52 shedding periods (corresponding to the present averaging period for the Re = 3900 cases) and ±6% for averaging over 120 periods (roughly corresponding to the number of periods that the Re = 13100 cases are averaged over). Norberg (1994) also reported on the sensitivity of the experimentally obtained L_r values to the spanwise length of the cylinder below 60D, while Lysenko et al. (2012) discussed the differences obtained by using Smagorinsky and TKE subgrid scale model in LES.

In the present study, $L_r = 1.27$ for the 3900_m4 case is in good agreement with previous LES of Breuer (1998 a), Franke and Frank (2002) and Tremblay (2002). Compared with the PIV measurements, the conclusions are similar to those drawn form velocity profiles in the cylinder wake. The present L_r values correspond better to the results of Lourenco and Shih (1993) and Dong et al. (2006) than to those of Parnaudeau et al. (2008).

Having in mind that the δ^+ value, i. e. the size of the smallest element at the cylinder surface,

the time-step, the domain size, the cylinder length and the spanwise grid resolution are kept constant, the sole influence of the grid is examined. Considering the good agreement with both numerical and experimental results, it is concluded that convergence is achieved for the 3900_m4 case, and that the chosen numerical model is suitable for simulating the flow in the subcritical regime.

TABLE 4: Hydrodynamic quantities – present and previous studies for Re = 3900.

Case	C_d	$C_{l\,rms}$	St	L_r
3900_m4	1.0784	0.1954	0.2152	1.27
Schlichting (1979)	1.0000		0.205 – 0.212	
Lourenco and Shih (1994)	0.99		0.22	1.19
Ong and Wallace (1996)	0.98±0.05		0.21	
Breuer (1998 a), Smagorinsky dynamic Smagorinsky	1.099 1.071		0.215±0.005	1.115, 1.197
Tremblay et al. (2002)	1.14		0.21	1.04
Franke and Frank (2002)	[0.978 – 1.005]		0.21	1.35
Dong et al. (2006)			0.2	1.36 – 1.47
Parnaudeau et al. (2008) PIV LES			 0.208±0.001	1.51
Lysenko et al. (2012) TKE and Smagorinsky	0.97 1.17		0.209 0.19	1.67 0.9

4. 3. FLOW AROUND THE CIRCULAR CYLINDER AT RE = 13100

For the flow around the circular cylinder at Re = 13100, eight simulations are carried out. Similar to the previous cases, the overall mesh characteristics are unchanged for all the simulations; the mesh resolution at the cylinder surface is kept nearly constant with $\delta^+ \leq 1$; and the boundary and the initial conditions are kept the same. Influences of several numerical parameters are investigated: the mesh refinement, the time-step, the domain width and the spanwise mesh resolution. The results are, after the convergence study, discussed through the integrated hydrodynamic quantities, the

velocity profiles in the cylinder wake, the recirculation length, the pressure distribution and the behaviour of the flow separation.

4. 3. 1. Hydrodynamic quantities

In the grid convergence study, four cases: 13100_m1, 13100_1, 13100_m2 and 13100_m3 are simulated varying the mesh density, with special attention paid to the near wake (Zones 1 and 2, Figure 2) while keeping the δ^+ value nearly constant. The influence of the mesh refinement is first analysed through the values of C_d, $C_{l\ rms}$ and St. Table 5 shows C_d and $C_{l\ rms}$ for the cases with varying mesh refinements. The mesh refinement from 7.6 million elements (13100_m2 case) to 11 million elements (13100_m3 case) results in less than 1% change of C_d and 6% change of $C_{l\ rms}$, while St obtains the same value for both simulations. This suggests that the finest mesh is sufficiently fine. To confirm that, further analysis of the mesh convergence study is presented in the following Section.

The influence of the time-step is also investigated through the C_d, $C_{l\ rms}$ and St values. The 13100_1, 13100_t2 and 13100_t3 cases are simulated with the same mesh (corresponding to the 13100_1 case), but by varying the time-step. Attention is paid to the Courant number, which mean value is always kept low and which maximum value (per mesh cell, per time-step) does not exceed 0.6. From Table 5, it is observed that the time-step variation does not have a strong influence on the results: the C_d variation is 1% between the cases with smallest and largest time-step, the $C_{l\ rms}$ variation is 5% and the St variation 1.4%. The dimensionless time-step of $0.001D/U_c$, used in all the latter cases, is therefore considered to be sufficiently small.

4. 3. 2. Flow in the cylinder wake

Velocities are sampled over the cross sections coinciding with the x-axis (x, z plane) and at the vertical cross section in the near wake (y, z plane) – consistent with what is chosen in Section 4.2.2. The pressure and the velocities are also sampled at the cylinder surface in order to observe the variations of C_p and the separation angle. The data is averaged over time and space in the same manner as before.

By comparing the streamwise velocity profiles in the cylinder wake, sampled in the (x, z) plane, y/D = 0 for the 13100_m1, 13100_1, 13100_m2 and 13100_m3 cases (Figure 8 a), it is found that the two simulations with the finest meshes give similar velocity values, while there are larger discrepancies for the 13100_m1 and 13100_1 cases. It can also be noticed that the finer meshes allow the cylinder wake to stretch farther in the wake region. That is supported by the fact that the coarsest mesh results in $L_r = 0.57$, while the other meshes yield larger values - 0.722 for the 13100_1 and 13100_m3 cases and a 6% longer L_r for the 13100_m2 case than the 13100_m3 case (see Figure 8 a). Similar effects are reported by Breuer (1998 b) and Tremblay et al. (2002); for the finer mesh cases, they describe farther propagating disturbances and better agreement with the experimental results (e. g. Lourenco and Shih, 1993).

A shorter wake, as simulated by the coarse mesh in the 13100_m1 case, leads to smaller velocities in the part of the wake where other three simulations still successfully capture the recirculation flow. This behaviour is depicted in Figure 8 b, showing that the streamwise mean velocity profile in the vertical (y, z) plane at x/D = 1.01 obtains a significantly less pronounced minimum than for the simulations with finer meshes. The results for the time- and space averaged C_p ($C_{p\,mean}$) distributions, presented in Figure 8 c, also show good agreement for the cases with finer meshes while the 13100_m1 case yields more negative values in the cylinder nape. Considering the

aforementioned behaviour of several flow characteristics, it is concluded that the mesh used in the 13100_m3 case has sufficiently fine grid resolution.

TABLE 5: Mean flow parameters for the Re = 13100 cases.

Case	C_d	$C_{l\,rms}$	St
13100_1	1.3509	0.6236	0.2038
13100_m1	1.3703	0.6750	0.2069
13100_m2	1.3013	0.5105	0.2038
13100_m3	1.3132	0.5454	0.2038
13100_t2	1.3358	0.6001	0.2038
13100_t3	1.3364	0.5879	0.2009
13100_sm	1.3433	0.6257	0.1980
13100_sl	1.3517	0.5788	0.2038

Other numerical effects are also investigated, such as the influence of the time-step, the spanwise mesh density and the spanwise length. Having in mind the large consumption of memory and CPU hours, simulations with even more mesh elements than the 13100_m3 case or with twice as large computational domain, and thus exceeding 20 million grid points, are demanding for the currently available computational resources. Therefore the analysis is made by comparison of the 13100_1 case to the cases with varying time-steps (13100_t2 and 13100_t3 cases), the spanwise refined mesh 13100_sm case and the elongated cylinder 13100_sl case (spanwise length 8D).

In Figure 9 a, the time- and space-averaged streamwise velocity component (u) profiles in the (x, z) plane are shown for the three simulations with different time-steps. Along the comparison of the hydrodynamic quantities in Section 4.3.1, behaviour of the wake flow is compared for the 13100_1, 13100_t2 and 13100_t3 cases. Figure 9 a leads to the conclusion that the time-steps used for these simulations are sufficiently small. A slight deviation in the streamwise mean velocity profile can be noticed between x/D = 1.5 and 3, but the difference is less than 3%. L_r for the three simulations obtains values between 0.674 and 0.722, which results in 3.5 % difference between the 13100_t3 and 13100_1 cases. The $C_{p\,mean}$ distributions for the cases with various time-steps are also

calculated. Similar to the behaviour of the previously analysed flow parameters, $C_{p\,mean}$ distributions for all three simulations have differences smaller than 2%. Therefore it can be concluded that the dimensionless time-step of 0.00013, used in simulation 13100_1 (and 13100_m2, 13100_m3, 13100_sl, 13100_sm) is sufficiently small.

Insufficient spanwise resolution could lead to large volumes of the individual elements and large aspect ratios of the element sides, which could cause numerical inaccuracies. In order to check the influence of the spanwise resolution, the 13100_1 and 13100_sm cases are simulated with the same (x, y) plane meshes, and changing the spanwise resolution from 100 to 150 elements per 4D cylinder length (Table 2). The results are: 0.5% difference in C_d, 3.7% difference in the $C_{l\,rms}$, and 1.5% difference in St. A more thorough analysis is made by comparing the near-wake streamwise velocity (u) profiles in (x, z) plane (Figure 9 b) and L_r. The differences are negligible. Therefore the spanwise distribution of 100 elements per 4D length of the cylinder is considered to be sufficient.

Another numerical aspect examined is the influence of the spanwise length of the domain. Most of the previous studies used a domain width of πD . A slightly wider domain of 4D is used for the majority of the present simulations. Nevertheless the common use of a smaller spanwise length, the question arises whether the 3D effects of the flow are fully captured. Breuer (1998 b) noticed significant differences between 2D and 3D simulations, and slight differences in the results for the simulations with πD and $2\pi D$ domain widths. Ouvrard et al. (2008) also discussed the importance of capturing the 3D effects of the flow, which was simulated fairly well even by using a relatively coarse mesh in the spanwise direction.

The 13100_sl case is simulated with the spanwise length of 8D with 200 elements in the z direction, keeping all the other numerical parameters the same as those used in the 13100_1 case. The differences between the hydrodynamic quantities are again very small. Figure 9 c shows the time- and space-averaged streamwise velocity component (u) in the horizontal (x, z) plane behind the cylinder. In the region between x/D = 2 and 4, a somewhat longer propagation of the

disturbance in the downstream direction is noticed for the 13100_sl case. The differences in the mean velocity profiles and L_r are insignificant, and thus the simulations with the spanwise length of 4D are considered acceptable.

4. 3. 3. Comparison with published experimental and numerical results

Following the conclusions from the convergence studies presented in the previous Sections, the 13100_m3 case is chosen for further analysis, through hydrodynamic quantities and flow properties in the cylinder wake. Table 6 summarizes the present and the previously published studies of hydrodynamic quantities for the flow around a circular cylinder at comparable and higher Re. For Re similar to the present study, published C_d values are between 1.0 (Cantwell and Coles, 1983) and 1.4 (Achenbach and Heinecke, 1981); St values between 0.188 (Fang and Han, 2011) and 0.215 (Cantwell and Coles, 1983). While there is limited published data for $C_{l\,rms}$, the present values of C_d and St are within these intervals.

TABLE 6: Hydrodynamic quantities, primary (Θ_1) and secondary separation angle (Θ_2) – present results for Re = 13100 and referred studies.

Case	C_d	$C_{l\,rms}$	St	Θ_1 (deg)	Θ_2 (deg)
13100_m3	1.3132	0.5454	0.2038	87.6	106
Roshko (1961) Re = 2.3 * 10^4	1.1250		0.19 (Ribner and Etkin, 1959)		
Son and Hanratty (1969) Re = 10^4, 2 * 10^4				96 97	118 115
Ballengee and Chen (1971) Re = 9.5 * 10^3, 1.7 * 10^4				92 88.5	
Achenbach and Heinecke (1981) Re = 2 * 10^4, (rough cylinder)	1.4		0.21		
Schewe (1983) Re = 2.3 * 10^4	1.1300	0.3200	0.1950		
Cantwell and Coles (1983) Re ~ 1.3 * 10^4	[1.0, 1.3]		[0.19-0.215]		
Norberg (1994) Re = 13000	0.98	0.04 – 0.15	0.20		
Breuer (1998 a) Re = 3900	[1.016-1.486]		0.22±0.005	[87.7-95.2]	[111.3-126]
Breuer (2000) Re = 1.4 * 10^5	[1.057-1.368]		[0.196-0.205]	[91.45-96.6]	
Ouvrard et al. (2008) Re = 1.4 * 10^5	[0.54-0.62]			[108-114]	
Ong et al. (2009) Re = 3.6 * 10^6	0.4574	0.0765	0.3052	114	
Fang and Han (2011) Re = 5.6 * 10^3, 2.8 * 10^4	[1.044-1.1] [1.029-1.127]		[0.188-0.195] [0.196-0.214]	[87-93] [98-105]	

The results of the 13100_m3 case are examined through the details of the velocity and pressure fields in the vicinity of the cylinder. There are neither numerical nor experimental results of the wake flow details for this Re. Therefore a qualitative comparison is made between the 13100_m3 case results and the previously published results for lower and higher Re. The comparison is made with the results for Re = 3900 by Lourenco and Shih (1993), Norberg (1994), Tremblay et al. (2000) and Lysenko et al. (2012), with both the numerical and experimental results for Re = 140000 by Breuer (2000), Cantwell and Coles (1983), and experimental studies with Re comparable with the present study by Thom (1928) and Lim and Lee (2002).

The velocity field in the cylinder wake is presented in Figure 10, through the time- and space-averaged streamwise velocity component (u) sampled in the (x, z) (Figure 10 a) and the (y, z) plane (Figure 10 b). In Figure 10 a, the velocity profile between x/D = 0.5 and x/D = 8 in the cylinder wake is compared with the Re = 3900 simulations of Tremblay et al. (2000) and Lysenko et al. (2012), the LES simulations of Breuer (2000) for Re = 140000 and the experimental data of Cantwell and Coles (1983) for Re = 140000. It appears that qualitatively all the results show similar behaviour in the cylinder wake. As reported in the previous research (e.g. Zdravkovich (1990)), an increase in Re leads to a shorter recirculation length. That causes the velocity minimum being located closer to the cylinder. This behaviour can be noticed in Figure 10 a, where the minimum velocity for the 13100_m3 case lies between the minima for the Re = 3900 and Re = 140000 simulations. This is also supported by comparison of the recirculation length. L_r for Re = 3900 is reported to be between 1.19 and 1.67 (Table 4); L_r = 1.27 for the 3900_m4 case. For the present Re = 13100, L_r is found to be 0.722 while for the higher Re, recirculation happens at about 0.5D behind the cylinder base (Cantwell and Coles, 1983).

Figure 10 b shows the streamwise velocity component sampled along the vertical cross sections located 1.01D behind the cylinder. Again, it appears that qualitatively the results are similar to the other numerical and experimental results, indicating the well-known V-shape velocity profile, similar to the one of the present Re = 3900 cases. As expected, due to the longer recirculation bubble than for higher Re, the profiles with lower Re yield more pronounced velocity minima at the cylinder centreline at x/D = 1.06. The results of the present study fall between the profiles for Re = 3900 and 140000, showing closer resemblance to the Re = 3900 flow. That is in agreement with the theory of Zdravkovich (1990) which gathers the flows in the Re range 2000 to 20000 (thus including Re = 3900 and Re = 13100) in the flow class with the transition vortices in the free shear layers, while the Re = 140000 flow falls into the next flow class with fully turbulent shear layers.

The $C_{p\ mean}$ distribution for the 13100_m3 case is presented in Figure 11. For the similar Re as in the present study, it is compared with the experimental results of Thom (1929) and Lim and Lee (2002), to both numerical and experimental results for lower Re = 3900 and to the experimental measurements for higher Re = 140000. Qualitatively, the pressure distribution follows the experimental and numerical results. Comparing the results for different Re, it can be noticed that with increasing Re, there is a trend of lower minima and more negative pressure at the lee side of the cylinder. Comparing the present results with Re = 3900, the trend has been captured. The absolute values of $C_{p\ mean}$ in the cylinder wake for the present study are, however, larger and the $C_{p\ mean}$ minimum is more pronounced than found by the investigations for both higher and lower Re. Krajnovic (2011), using LES of the flow around the finite cylinder at Re = 20000, and Lysenko et al. (2012) presenting the LES with Smagorinsky model for the compressible flow at Re = 3900, also report the lower $C_{p\ mean}$ minima than observed in the experiments by Norberg (1994). Based on these results, a more thorough analysis should be made to investigate the influence of the Smagorinsky subgrid scale model on the results.

Another flow parameter examined is the position of the separation point on the cylinder surface. Relying on the definition of the separation point as the point of zero shear stress, it is calculated as a point of zero tangential velocity at the first mesh node next to the cylinder surface. The time-averaged velocity components in the streamwise (u) and the crossflow (v) direction are calculated and sampled at each mesh cell. The precision is therefore, for the 13100_m3 case with 540 elements distributed circumferentially, 0.67º. The separation angle is analysed through its spanwise-averaged values.

Previously published results for the position of the separation point at comparable Re are scarce and the results are highly varying. Therefore the present results for Re = 3900 are first compared with previous results for the same Re, while the Re = 13100 results are compared with results from studies for both higher and lower Re. Two separation angles are detected. The smaller

angle, Θ_1 (measured from the cylinder vertex clockwise for the upper and counter-clockwise for the lower half of the cylinder) determines the primary separation point. For the 3900_m4 case, Θ_1 = 86.4º. That value compares very well with the PIV measurements of Lourenco and Shih (1993), as well as with the LES results of Breuer (1998 b), Parnaudeau et al. (2008) and Lysenko et al. (2012) for Smagorinsky and TKE model, reporting Θ_1 = 86º; 87º; 86º; 89º and 88º respectively.

Similarly, for the 13100_m3 case, two separation points are present; Θ_1 = 87.6º and Θ_2 = 106º. For comparable Re, Ballengee and Chen (1971) presented Θ_1 = 92º for Re = 9.5 * 10^3 and Θ_1 = 88.5º for Re = 1.7 *10^4; Fang and Han (2011) found Θ_1 between 87º and 93º for Re = 5.6 * 10^3 and between 98º and 105º for Re = 2.8 * 10^4. According to Achenbach (1968), the position of the separation point depends on Re. For the subcritical flow, the separation point is expected to move downstream as Re increases, resulting in an increase of Θ_1. The increase is relatively small, with Θ_1 varying between 75º and 95º in the subcritical flow regime, followed by a sudden jump due to transition to the critical flow, at Re about 3*10^5, and a slight decrease in the supercritical flow regime, at Re about 10^6. Accordingly, the present Θ_1 result (87.6º) is in good agreement with the theory, giving a slightly larger value than reported for Re = 3900, similar values as the aforementioned comparable Re and a smaller angle than obtained for higher Re (see Table 6).

Continuing downstream from the primary separation point, a small counter-rotating vortex is detected for both Re = 3900 and Re = 13100 simulations in the present studies. Figure 12 shows the time-averaged streamlines in the (x, y) plane, cross section at z/D = 2 for the 13100_m3 case. Small vortices are symmetrically located on both sides of the cylinder, extending over about 18 º behind the primary separation point. Similar vortices were observed by Son and Hanratty (1969) for Re = 10^4 and 2 * 10^4, spanning over approximately 25º. Breuer (1998 a) and Lysenko et al. (2012) captured the secondary circulation by LES for Re = 3900, covering about 25º behind Θ_1.

5. CONCLUSIONS

The flow around a circular cylinder in a uniform incoming flow for intermediate and moderately high Reynolds numbers is investigated using LES with Smagorinsky subgrid scale turbulence closure. The numerical code OpenFOAM is used for all simulations. The validation is carried out through the benchmark case of the flow around a circular cylinder at Re = 3900. The results are analysed through the hydrodynamic values of drag and lift coefficients and through the flow profiles in the near wake of the cylinder. Good agreement is obtained between the present results and the results from previously published studies, carried out with various numerical models, such as LES and DNS, as well as by experiments. The LES with Smagorinsky turbulence closure performs well in the studied subcritical flow regime.

The same numerical model is further used to simulate the flow at higher Re in the subcritical flow regime, Re = 13100. The influences of the different numerical parameters are investigated, such as mesh refinement, time-step, and cylinder spanwise length, with emphasis on the influences of the boundary conditions. The results are examined through the hydrodynamic quantities C_d, $C_{l\,rms}$, and St, the distribution of $C_{p\,mean}$ on the cylinder surface, the velocity distribution in the cylinder wake, the recirculation length and the separation angle. Since there are no publications of the flow details for the present Re, the results are compared qualitatively with published results for the same flow regime.

The main findings are:

– Even for the meshes with fine resolution on the cylinder surface ($\delta^+ < 1$), the mesh resolution in the cylinder near wake has a significant effect on the results.

– Since the flow in the chosen regime is 3D, the domain, and thus the cylinder length, should be chosen such that it captures the 3D flow effects. It is concluded that a domain width of 4D is

sufficient.

- High spanwise mesh resolution does not change the results significantly.
- The results are not very sensitive to the choice of the time-step, as long as the Courant number is kept reasonably low.
- With increasing Re, the trend of shortening of the recirculation length is captured, as well as the trend of increasing separation angle.
- A small recirculation vortex is captured, extending over approximately 20º behind the primary separation point.

In general, the results for the flow parameters are in reasonably good agreement with previous research. The pressure and the velocity distributions on the cylinder surface and in the near wake show good agreement with the previous experimental results. Comparison with the previous numerical results for lower and higher Re shows good qualitative agreement, following the previously documented trends. Therefore it appears that LES are suitable for the flow in the chosen flow regime.

ACKNOWLEDGEMENT

This work has been supported by the Norwegian University of Science and Technology. Computing time, supported by NOTUR (the Norwegian Metacenter for Computational Science) is granted by the Norwegian Research Council and the Norwegian University of Science and Technology. This support is gratefully acknowledged. We are grateful to Tufan Arslan for technical support and valuable discussions.

REFERENCES

Achenbach, E., 1968. Distribution of local pressure and skin friction in cross flow around a circular cylinder up to Re = 5 * 10^6. Journal of Fluid Mechanics. 34, 625-39.

Achenbach, E., Heinecke, E., 1981. On vortex shedding from smooth and rough cylinders in the range of Reynolds numbers 6 x 10^3 to 5 x 10^6. Journal of Fluid Mechanics. 109, 239-251.

Ballengee, D. W., Chen, C. F., 1971. Experimental determination of the separation point of flow around the circular cylinder. Published in Zdravkovich, M. M., 1997. Flow Around Circular Cylinders, Vol 1: Fundamentals. Oxford University Press, Oxford, UK.

Breuer, M., 1998 a. Numerical and modeling influences on large eddy simulations for the flow past a circular cylinder. International Journal of Heat and Fluid Flow. 19, 512-521.

Breuer, M., 1998 b. Large eddy simulation of the subcritical flow past a circular cylinder: numerical and modeling aspects. International Journal for Numerical Methods in Fluids. 28, 1280-1302.

Breuer, M., 2000. A challenging case for large eddy simulation of high Reynolds number circular cylinder flow. International Journal of Heat and Fluid Flow. 21, 648-654.

Cantwell, B., Coles, D., 1983. An experimental study of entrainment and transport in the turbulent near wake of a circular cylinder. Journal of Fluid Mechanics. 136, 321-374.

Catalano, P., Wang, M., Iaccarino, G., Moin, P., 2003. Numerical simulation of the flow around a circular cylinder at high Reynolds numbers. International Journal of Heat and Fluid Flow. 24, 463-469.

Diana, G., Belloli, M., Giappino, S., Muggiasca, S., 2008. Vortex induced vibrations at high Reynolds numbers. BBAA VI International Colloquium on: Bluff Bodies Aerodynamics & Applications, Milano, Italy.

Fang, Y., Han, Z., 2011. Numerical experimental research on the hydrodynamic performance of flow around a three dimensional circular cylinder. Applied Mechanics and Materials. 90-93, 2778-2781.

Ferziger, J. H., Peric, M., 2001. Computational Methods for Fluid Dynamics, 3rd Ed. Springer-Verlag, Berlin, Germany.

Franke, J., Frank, W., 2002. Large eddy simulation of the flow past a circular cylinder at Re_D = 3900. Journal of Wind Engineering and Industrial Aerodynamics. 90, 1191-1206.

Germano, M., Piomelli, U., Moin, P., Cabbot, W. H., 1991. A dynamic subgrid scale eddy viscosity model. Physics of Fluids A. 3 (7), 1760-1765.

Heggernes, K., 2005. Numerical Simulation of Three-dimensional Viscous Flow Around Marine Structures,

Doctoral Thesis. Norwegian University of Science and Technology. 2005:170.

Krajnovic, S., 2011. Flow around a tall finite cylinder explored by large eddy simulation.. Journal of Fluid Mechanics, 676, 294-317.

Li, Y., 2011. Large eddy simulation of flow around a cylinder at Re=3900 using a CFD code. Applied Mechanics and Materials. 94-96, 1707-1710.

Lilly, D. K., 1992. A proposed modification of the Germano subgrid-scale closure method. Physics of Fluids A. 4 (3), 633 – 635.

Lim, H. C., Lee, S. J., 2002.Flow control of circular cylinders with longitudinal grooved surfaces. AIAA Journal, 40, 10, 2027-2036.

Lin, Z., Zhao, D., Song, J., 2011. The influence of advection schemes and turbulence closure models on drag coefficient calculation around a circular cylinder at high Reynolds number. Journal of Ocean University of China (Oceanic and Coastal Sea Research). 10 3, 229-233.

Linke, W., 1931. New measurements on aerodynamics of cylinders, particularly their friction resistance (in German). Physichalishce Zeitschrift. 32, 900 – 14. Published in Zdravkovich, M. M., 1997. Flow Around Circular Cylinders, Vol 1: Fundamentals. Oxford University Press, Oxford, UK.

Lourenco, L. M., Shih, C., 1993. Characteristics of the plane turbulent near wake of a circular cylinder, a particle image velocimetry study. Published in Beaudan, P., Moin, P., 1994. Numerical experiments on the flow past a circular cylinder at sub-critical Reynolds number. Report no. TF-62, Thermosciences Division, Department of Mechanical Engineering, Stanford University, USA.

Lysenko, D. A., Ertesvåg, I. E., Rian, K. E,, 2012. Large-eddy simulation of the flow over a circular cylinder at Reynolds number 3900 using the OpenFOAM toolbox. Flow Turbulence Combust. 89:491-518.

Norberg, C., 1994. An experimental investigation of the flow around a circular cylinder: investigation of the aspect ratio. Journal of Fluid Mechanics. 258, 287-316.

Ong, L., Wallace, J., 1996. Velocity field of the turbulent very near wake of a circular cylinder. Experiments in Fluids. 20, 441-453.

Ong, M. C., Utnes, T., Holmedal., L. E., Myrhaug, D., Pettersen, B., 2009. Numerical simulation of flow around a smooth circular cylinder at very high Reynolds numbers. Marine Structures. 22, 142-153.

OpenFOAM, 2011. The open source CFD toolbox, programmer's guide, version 2.1.0. OpenFoam Foundation. Accessible 21.9.2012. on: http://www.scribd.com/doc/80373296/UserGuide.

Ouvrard, H., Koobus, B., Salvetti, M-V., Camarri, S., Dervieux, A., 2008. Variation multiscale LES and hybrid

RANS/LES parallel simulation of complex unsteady flows. VECPAR 2008. Ed: Palma, J. M. L. M. et al. Springer-Verlag, Berlin. LNCS 5336, 465-478.

Parnaudeau, P., Carlier, J., Heitz, D., Lamballais, E., 2008. Experimental and numerical studies of the flow over a circular cylinder at Reynolds number 3900. Physics of Fluids. 20, 085101.

Ribner, H. S., Etkin, B., 1959. Noise research in Canada. Procedings of the 1st International Congress of Aero. Sci, Madrid. Published by Pergamon Press, London, UK.

Roshko, A., 1961. Experiments on the flow past a circular cylinder at very high Reynolds numbers. Journal of Fluid Mechanics. 10, 345-356.

Schewe, G., 1983. On the force fluctuations on a circular cylinder in crossflow from subcritical up to transcritical Reynolds numbers. Journal of Fluid Mechanics. 133, 265-285.

Schlichting, H., 1979. Boundary Layer Theory. McGraw Hill Inc, USA.

Smagorinsky, J., 1963. General circulation experiments with the primitive equations. Monthly Weather Review. 91-3, 99-164.

Son, J. S., Hanratty, T. J., 1969. Velocity gradients at the wall for flow around a cylinder at Reynolds numbers from 5k to 100k. Journal of Fluid Mechanics. 35, 353-68.

Thom, A., 1928. An investigation of fluid flow in two-dimensions. Aeronautical Research Council, Reports & Memoranda 1194 (Th. Numerical Calc.).

Tremblay, F., Manhart, M., Friedrich, R., 2000. DNS of flow around the circular cylinder at subcritical Reynolds number with Cartesian grids. Proceedings of the 8th European Turbulence Conference, EUROMECH, Barcelona, Spain. 659-662.

Tremblay, F., Manhart, M., Friedrich, R., 2002. LES of flow around a circular cylinder at a subcritical Reynolds number with Cartesian grids. Advances in LES of Complex Flows. Kluwer Academic Publishers, Netherlands. 133-150.

Vaz, G., Mabilat, C., van der Wal, R., Gallagher, P., 2007. Viscous flow computations on smooth cylinders, a detailed numerical study with validation. Proceedings of the 26th International Conference on Offshore Mechanics and Arctic Engineering, San Diego, California. OMAE2007-29275.

Weller, H. G., Tabor, G., Jasak, H., Fureby, C., 1998. A tensorial approach to computational fluid continuum mechanics using object-oriented techniques. Computers in Physics. 12-6, 620-631.

Wissink, J. G., Rodi, W., 2008. Large-scale computations of flow around a circular cylinder. Published in Resch, M., Roller, S., Lammers, P., Furui, T., Galle, M., Bez, W. 2008. High Performance Computing on Vector

Systems. Springer-Verlag, Berlin Heidelberg, Germany.

Zdravkovich, M. M., 1990. Conceptual overview of laminar and turbulent flows past smooth and rough circular cylinders. Journal of Wind Engineering and Industrial Aerodynamics. 33, 53-62.

Zhang, J., Dalton, C., 1996. Interactions of vortex-induced vibrations of a circular cylinder and a steady approach flow at a Reynolds number of 13,000. Computers and Fluids. 25-3, 283-294.

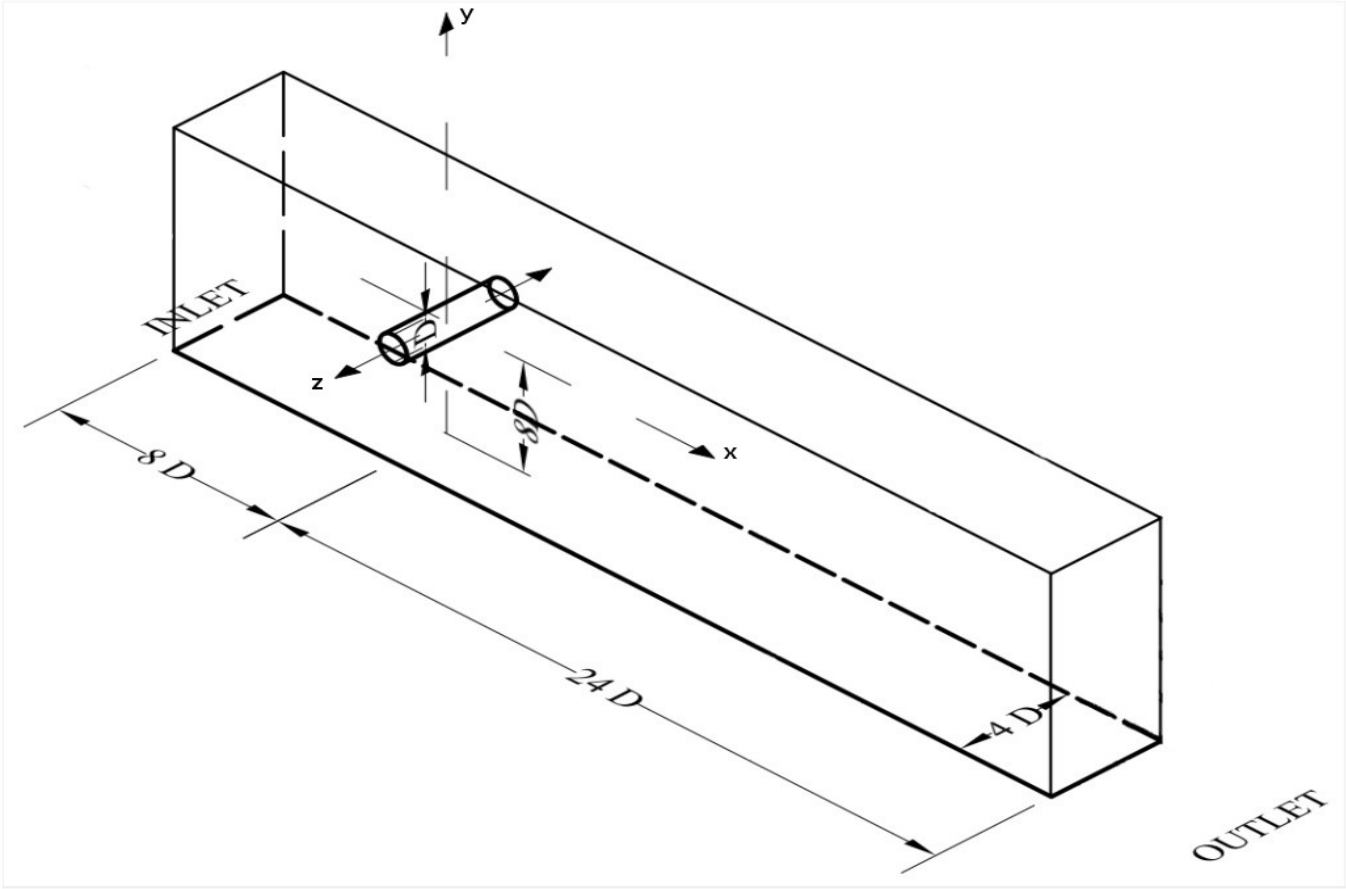

FIGURE 1: The computational domain.

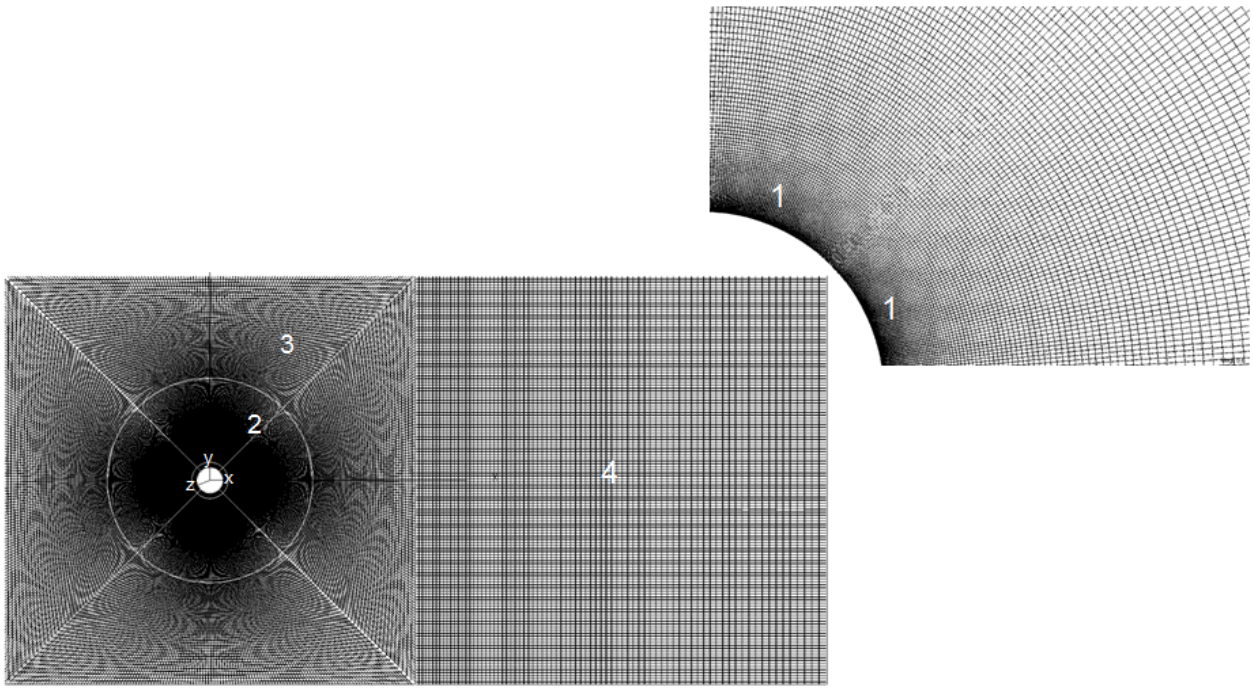

FIGURE 2: Visualization of the mesh – Zones 2, 3 and 4 and Zone 1 in the immediate vicinity of the cylinder. Zones and the coordinate system are shown.

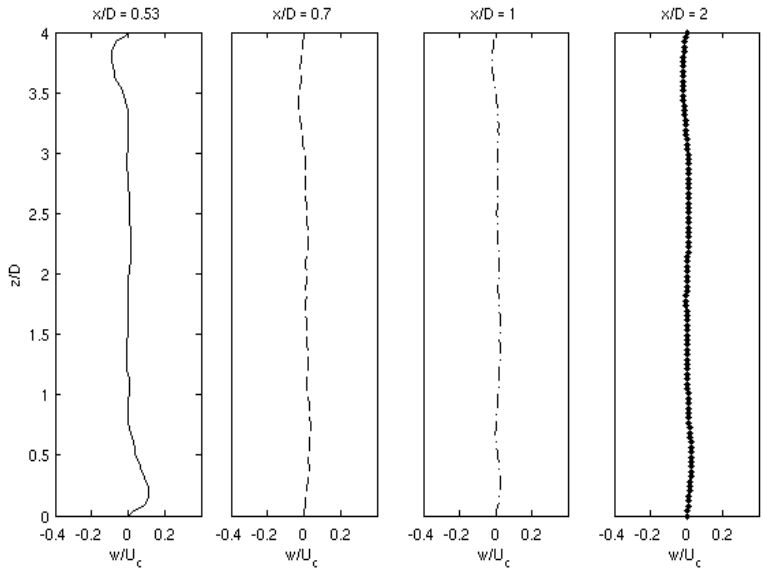

FIGURE 3: Time-averaged wall-normal velocity component (w) at four cross sections in the cylinder wake, 13100_1 case.

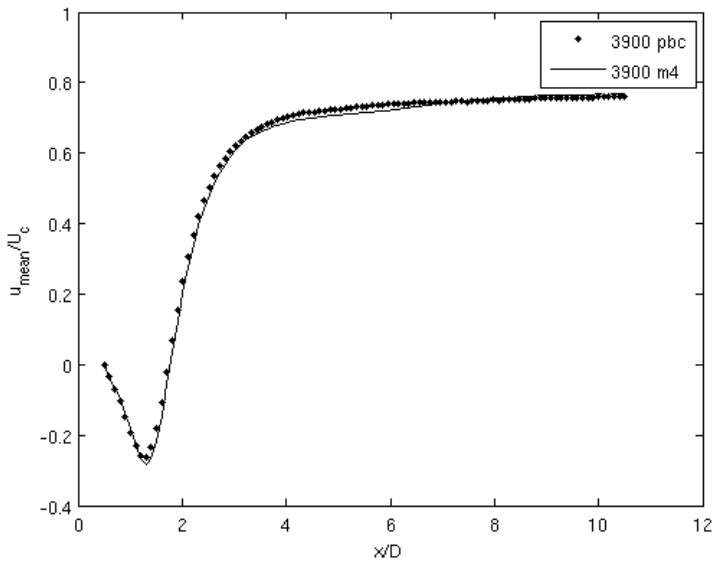

FIGURE 4: Time- and space-averaged streamwise velocity component (u) profile in the cylinder wake, in the (x, z) plane, y = 0 for the 3900_m4 case with the free-slip boundary condition and 3900_pbc case with the periodic boundary condition.

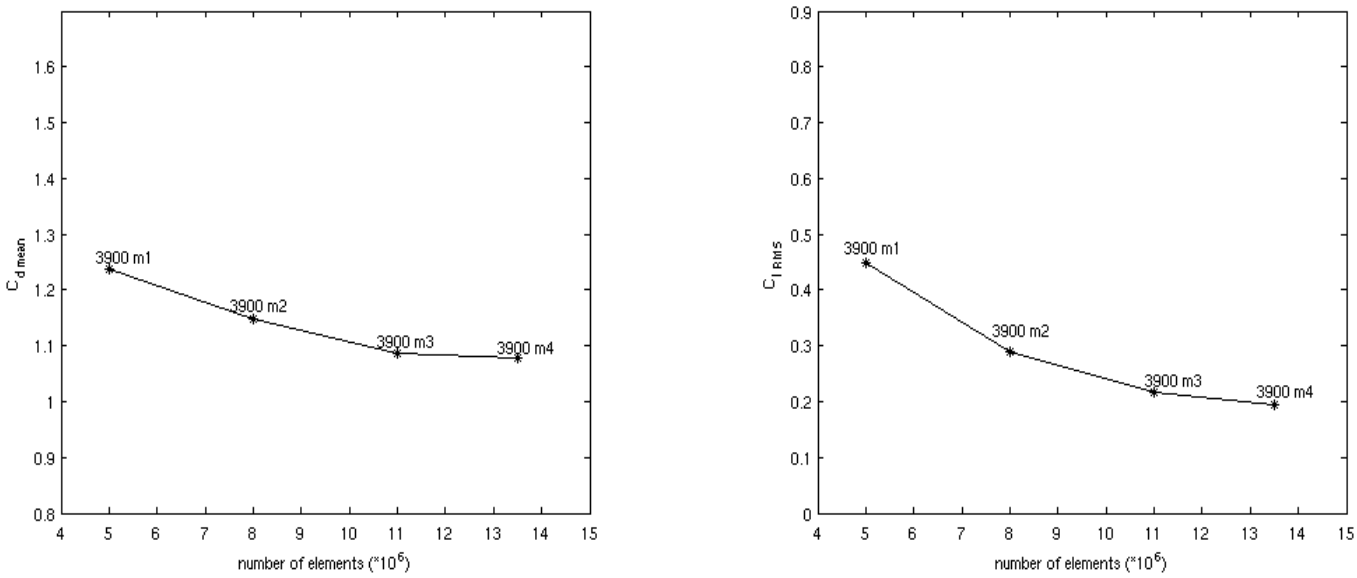

FIGURE 5: C_d and $C_{l\,rms}$ versus the number of elements for Re = 3900. Cases: 3900_m1, 3900_m2, 3900_m3, 3900_m4.

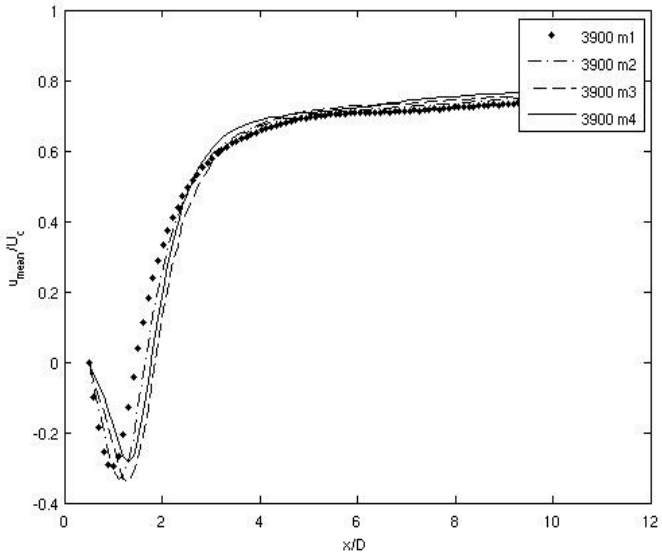

FIGURE 6: Time- and space-averaged streamwise velocity component (u) profile in the cylinder wake, in the (x, z) plane at y = 0.

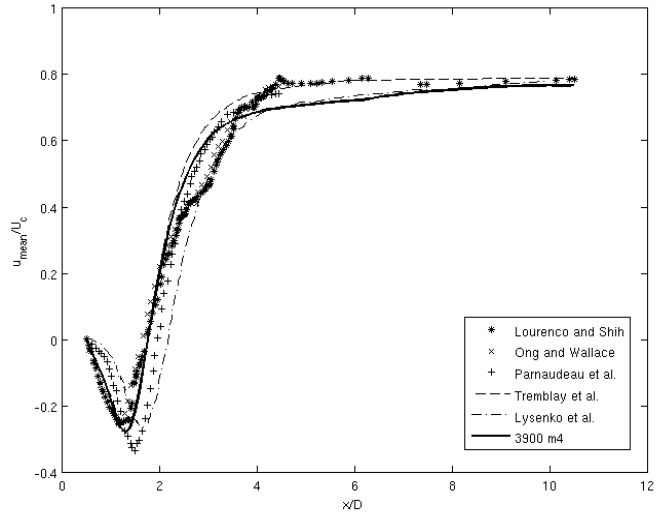

a)

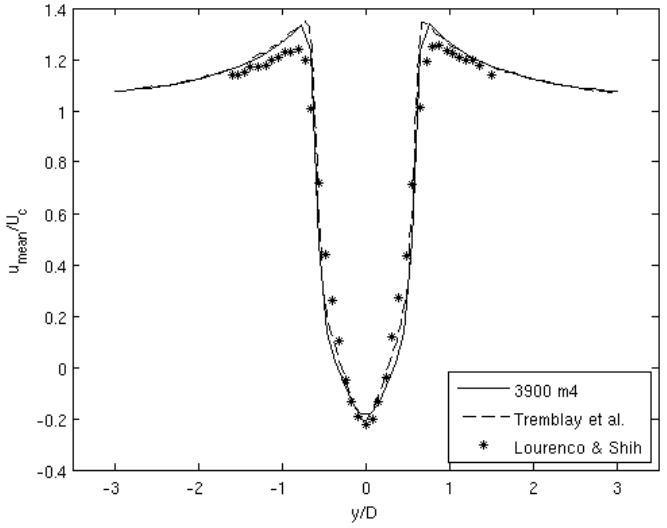

b)

FIGURE 7: Time- and space-averaged streamwise velocity component (u) profile in the cylinder wake

a) in the (x, z) plane, y = 0. Experimental results by Lourenco and Shih (1993), Ong and Wallace (1996) and Parnaudeau et al. (2008), DNS simulation by Tremblay et al. (2000) and LES simulation by Lysenko et al. (2012), present study - 3900_m4 case.

b) in the (y, z) plane, x = 1.06. Present study - 3900_m4 case, DNS results by Tremblay et al. (2000), experimental results by Lourenco and Shih (1993).

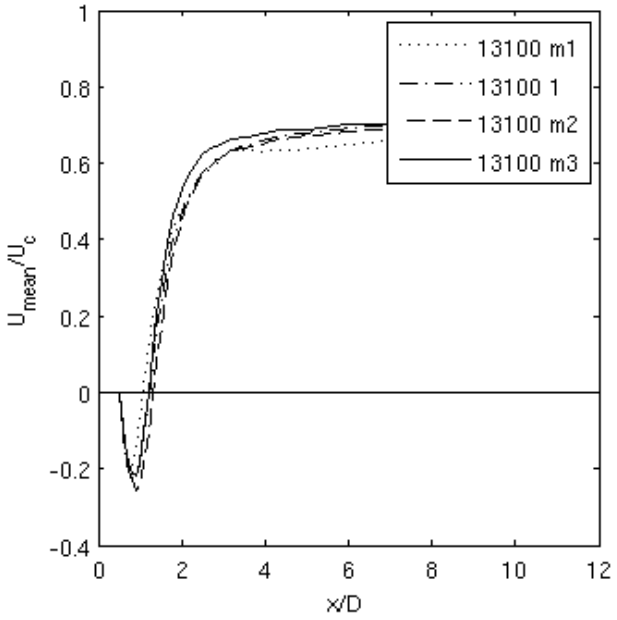

a)

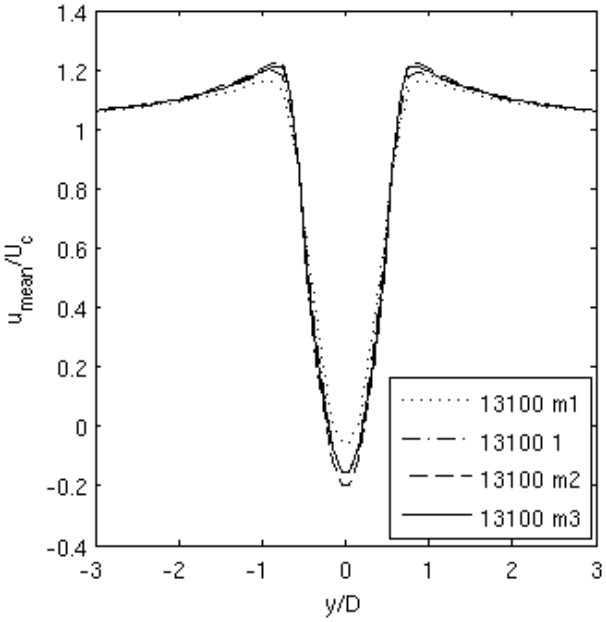

b)

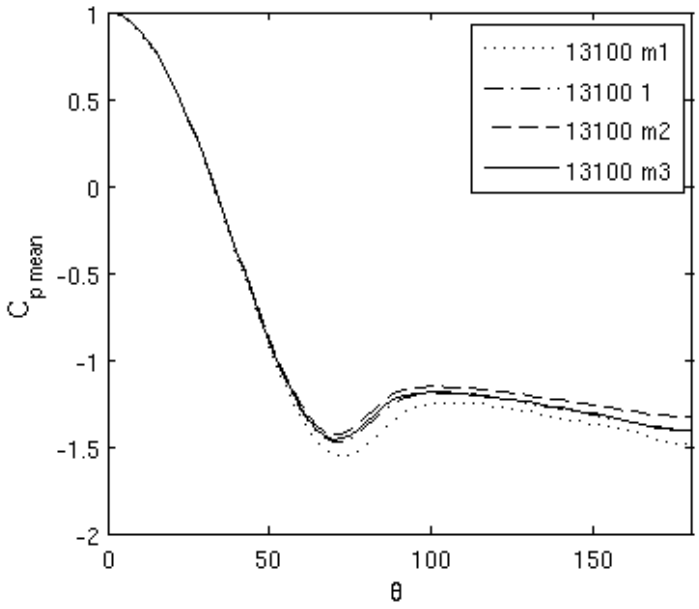

c)

FIGURE 8: Time- and space-averaged flow properties for the Re = 13100 cases with varying number of elements

a) streamwise velocity component (u) profile in the cylinder wake, in the (x, z) plane, y = 0;

b) streamwise velocity component (u) profile in the cylinder wake, in the (y, z) plane, y = 1.01;

c) $C_{p\,mean}$ distribution around the cylinder surface. Θ is measured from the cylinder front clockwise for the upper and anticlockwise for the lower half of the cylinder.

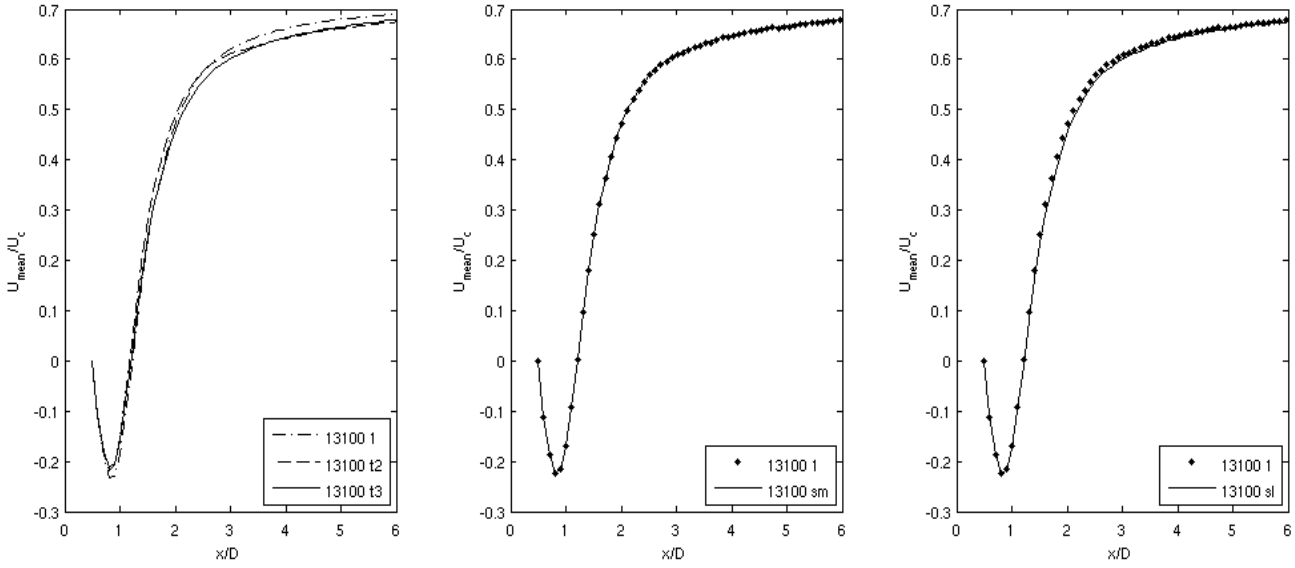

a) b) c)

FIGURE 9: Time- and space-averaged streamwise velocity component (u) profiles in the cylinder wake, in the (x, z) plane, y = 0

a) versus the time-step;

b) versus the mesh resolution in the spanwise direction;

c) versus the cylinder spanwise length.

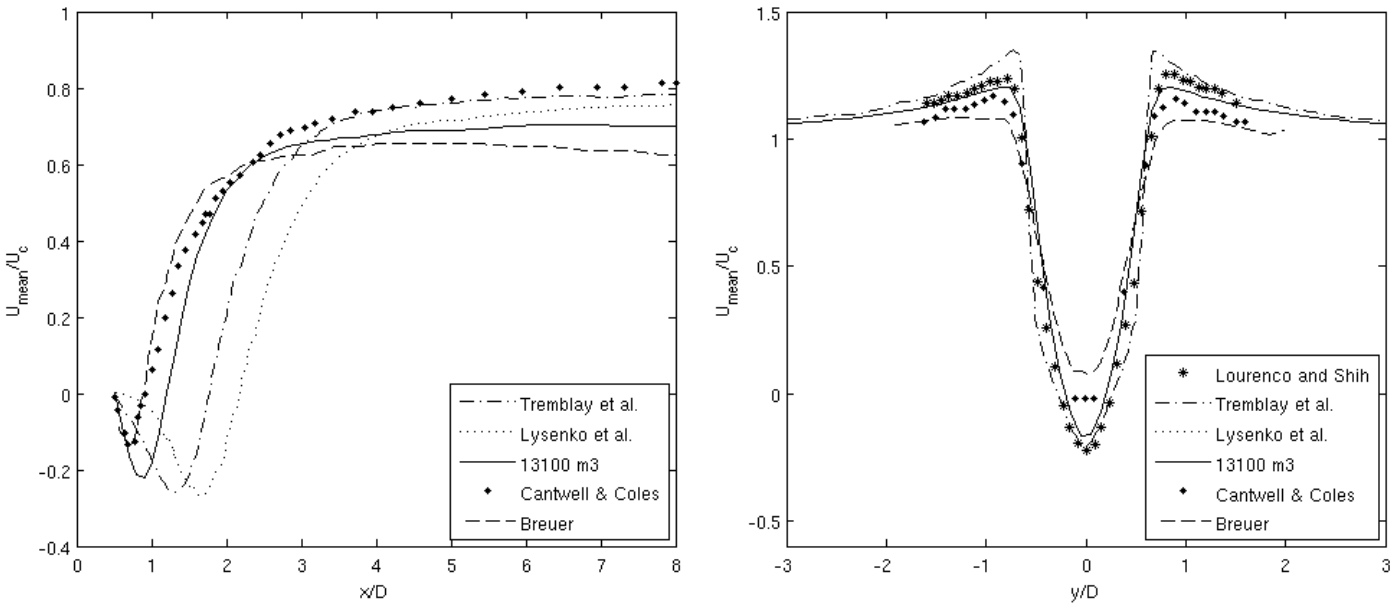

a) b)

FIGURE 10: Time- and space-averaged streamwise velocity component (u) profiles in the cylinder wake

a) in (x, z) plane, y/D = 0;

b) in (y, z) plane, x/D = 1.06.

Symbols:

Re = 3900, * Lourenco and Shih (1993); -.- Tremblay et al. (2000); … Lysenko et al. (2012);

Re = 13100, — 13100_m3 case;

Re = 140000, • Cantwell and Coles (1983); Breuer (2000).

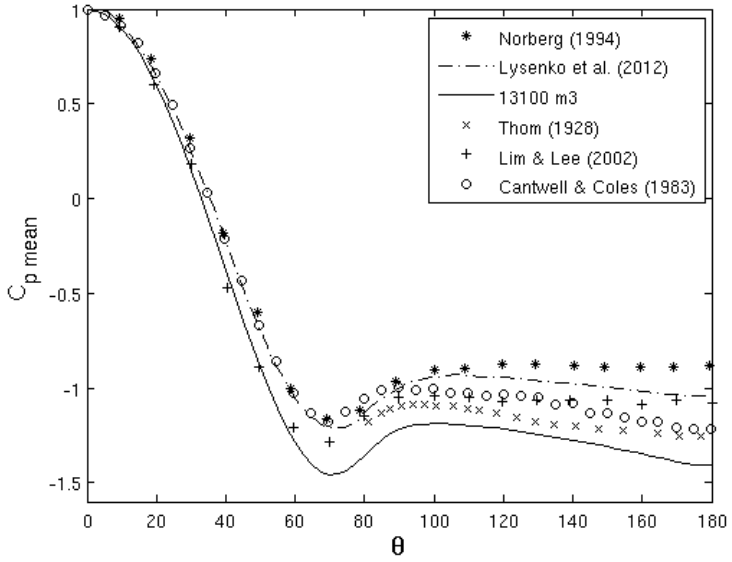

FIGURE 11: Time- and space-averaged $C_{p\,mean}$ distribution around the cylinder.

Re = 3900, Norberg (1994) and Lysenko (2012);

Re = 13100, case 13100_m3;

Re = 16700, Thom (1929);

Re = 24000, Lim and Lee (2002);

Re = 140000, Cantwell and Coles (1983).

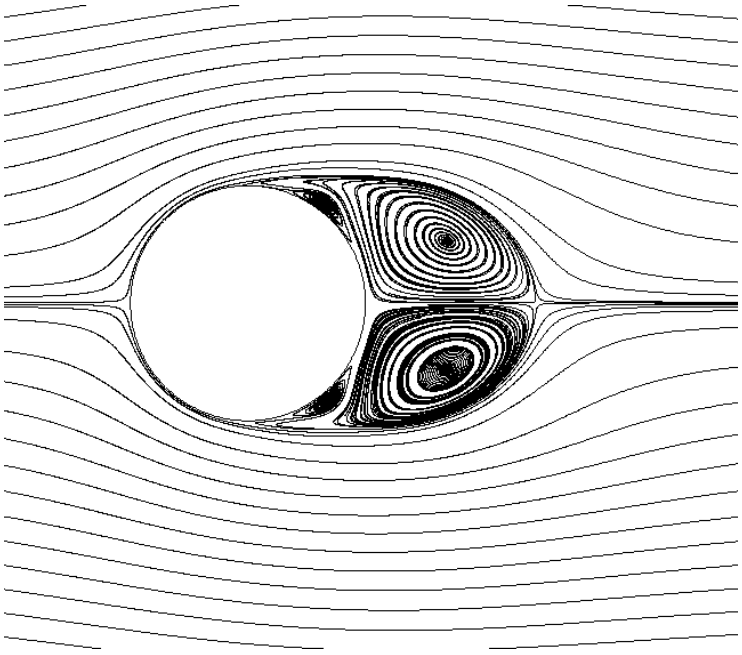

FIGURE 12: Time-averaged streamlines in the (x, y) plane, cross section at z/D = 2; 13100_m3 case. Primary and secondary separation can be seen.